

Quantum extraordinary-log universality of boundary critical behavior

Yanan Sun¹ and Jian-Ping Lv^{1,*}

¹*Department of Physics and Anhui Key Laboratory of Optoelectric Materials Science and Technology,
Key Laboratory of Functional Molecular Solids, Ministry of Education,
Anhui Normal University, Wuhu, Anhui 241000, China*

(Dated: May 3, 2022)

Recent discovery of the extraordinary-log universality has generated tremendous interest in classical and quantum boundary critical phenomena. However, the classical-quantum correspondence of such a universality remains elusive. Here, by utilizing quantum Monte Carlo simulations, we study the quantum edge criticality of a two-dimensional Bose-Hubbard model featuring emergent bulk criticality. On top of an insulating bulk, the open edges experience a Kosterlitz-Thouless-like transition into superfluid phase when sufficiently enhancing the hopping strength on edges. At the bulk critical point, the edges exhibit the special, the ordinary and the extraordinary critical phases. In the extraordinary phase, logarithms are involved in the finite-size scaling of two-point correlation and superfluid stiffness, which admit a classical-quantum correspondence for the extraordinary-log universality. Thanks to the modern quantum emulator for interacting bosons in lattices, the edge critical phases might be realized in experiments.

Keywords: boundary critical behavior; extraordinary-log critical phase; universality class; Monte Carlo; quantum emulator

Introduction. Boundary critical behavior (BCB) refers to the critical phenomena occurring on boundaries of a critical bulk [1–12]. Due to the fundamentality of BCB, it closely connects to a rich variety of modern concepts including symmetry protected topological phase [13–15], Casimir effect [16] and boundary conformal field [17–19].

Recently, the extraordinary-log universality (ELU) of BCB was predicted for the classical three-dimensional (3D) $O(N)$ model with $2 \leq N < N_c$, where N_c was unknown [20]. The ELU features that the boundary two-point correlation $g(r)$ decays logarithmically with the spatial distance r as [20]

$$g(r) \sim [\ln(r)]^{-\hat{\eta}}, \quad (1)$$

where $\hat{\eta}$ is only dependent of N . This prediction dramatically differs from the paradigm of criticality, where $g(r)$ exhibits the power-law decay [21–24]

$$g(r) \sim r^{2-(d+z)-\eta} \quad (2)$$

with η the anomalous dimension, d the spatial dimension and z the dynamic critical exponent. Shortly after the prediction of ELU [20], much attention was devoted to the BCB in classical [25–31] and quantum [32–36] systems.

Evidence for the ELU was obtained from the Monte Carlo simulations of classical Heisenberg and XY models [25, 26, 28]. A conformal bootstrap study took N as a continuous parameter and yielded $N_c \approx 5$ [27]. An alternative scaling formula of $g(r)$ was conjectured [26] based on the Monte Carlo data of XY model, where the critical magnetic fluctuations at zero and smallest non-zero modes scale as $L^2[\ln(L)]^{-\hat{q}}$ and $L^2[\ln(L)]^{-\hat{\eta}}$, with the critical exponents \hat{q} and $\hat{\eta} = \hat{q} + 1$, respectively. This observation can be related to the finite-size scaling (FSS) of $g(r)$ as [26]

$$g(r) \sim \begin{cases} [\ln(r)]^{-\hat{\eta}}, & \ln(r) \leq \mathcal{O}[(\ln(L))^{\hat{q}/\hat{\eta}}], \\ [\ln(L)]^{-\hat{q}}, & \ln(r) \geq \mathcal{O}[(\ln(L))^{\hat{q}/\hat{\eta}}]. \end{cases} \quad (3)$$

The two exponents were also observed for the classical ELU at an emergent $O(2)$ critical point [30]. Eq. (3) formally agrees with (1) on the FSS of $g(r)$ in the $r \rightarrow \infty$ limit.

Assuming that the classical-quantum correspondence exists, the universality of 3D classical $O(N)$ BCB may be realized by the quantum edge criticality (QEC) in two dimensions. Hitherto, 2D QEC has been extensively studied in the context of 2D dimerized antiferromagnetic quantum (2D-DAQ) models with Heisenberg and XXZ spins, which are prototype models for quantum $O(3)$ and $O(2)$ critical phenomena [9–12, 32–34], respectively. On one hand, the dangling edges of 2D-DAQ spin-1/2 and spin-1 Heisenberg models harbor a non-ordinary edge criticality [10–12, 32], which differs from the $O(3)$ ordinary BCB. Instead, the critical exponents in magnetic sector are close to those of the $O(3)$ special transition [10, 11]. In Ref. [32], the numerical result of scaling dimension Δ_n (Δ_v) for Néel (valence bond solid) order was compared to the field-theoretic prediction [37]

$$\begin{aligned} \Delta_n - 1/2 &= \epsilon_n \\ \text{and } \Delta_v - 1/2 &= -3\epsilon_n \end{aligned} \quad (4)$$

with $\Delta_\phi - 3/2 = -\epsilon_n$, where $\Delta_\phi \approx 1.187$ [6] is the scaling dimension for spin order in the $O(3)$ ordinary universality. For the spin-1/2 case, numerical results do not fully agree with Eq. (4) and merely conform with the scaling relation $3\Delta_n + \Delta_v = 2$. For the spin-1 case, the estimate $\Delta_v \approx -2$ is roughly compatible with the theory of novel extraordinary-power phase [20], hence in sharp contrast to Eq. (4) and inconsistent with the ELU as indicated by the classical Heisenberg BCB [25]. On the other hand, the non-dangling edges of 2D-DAQ spin-1/2 Heisenberg model host the ordinary phase, the special transition and the *long-range ordered* extraordinary phase [10, 11, 33]. Moreover, the 2D-DAQ spin-1 XXZ model may exhibit the extraordinary-log criticality [34], for which the estimate of \hat{q} is roughly compatible to that of classical XY model given in Ref. [26]. However, this estimate does not hold for the spin-1/2 case [34].

As indicated in Ref. [20], the existing results had not

* jplv2014@ahnu.edu.cn

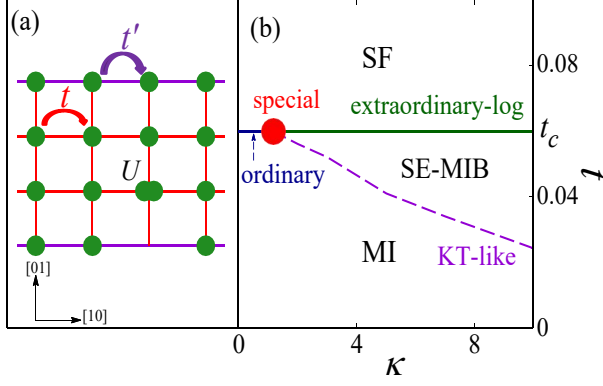


Figure 1. Model and ground-state phase diagram. (a) Definition of open-edge Bose-Hubbard model, where t and t' are hopping amplitudes and U denotes onsite repulsion. (b) The phase diagram in terms of t and the edge hopping enhancement κ , includes a phase with superfluid edges and Mott insulating bulk (SE-MIB) as well as the phases of bulk-edge superfluid (SF) and Mott insulator (MI). These phases are separated by the Kosterlitz-Thouless-like (KT-like), the extraordinary-log and the ordinary critical lines that are terminated at the multi-critical special transition point.

formed a self-contained picture for the quantum extraordinary phases. Realization of classical-quantum correspondence for the ELU is still awaited. Here, we exploit the BCB of interacting bosons by a 2D Bose-Hubbard model and show that the model is a candidate for quantum ELU. We draw this conclusion not only by the logarithmic FSS of two-point correlation and superfluid stiffness for the extraordinary phase, like that in classical statistical models [20, 25, 26], but also by an overall classical-quantum correspondence for a rich variety of critical phases.

Model and ground-state phase diagram. We consider the square-lattice Bose-Hubbard model at unit boson filling with the Hamiltonian

$$\hat{H} = - \sum_{\langle ij \rangle} t_{ij} (\hat{b}_i^\dagger \hat{b}_j + \hat{b}_j^\dagger \hat{b}_i) + \frac{U}{2} \sum_i \hat{n}_i (\hat{n}_i - 1), \quad (5)$$

where \hat{b}_i^\dagger and \hat{b}_i are respectively bosonic creation and annihilation operators at site i , and $\hat{n}_i = \hat{b}_i^\dagger \hat{b}_i$. t_{ij} denotes the amplitude of the nearest-neighbor hopping between i and j , and $U > 0$ represents onsite repulsion. The first summation runs over nearest neighboring sites while the second summation is over sites. We set $U = 1$ as energy unit.

As illustrated by Fig. 1(a), we define our model for BCB by setting open and periodic boundary conditions along [01] and [10] directions, respectively. Hence, a pair of open edges are specified. The hopping amplitude $t_{ij} = t'$ on open edges is distinguished from $t_{ij} = t$ in bulk. The edge hopping enhancement is parameterized by $\kappa = (t' - t)/t$.

At $\kappa = 0$, model (5) reduces to the standard Bose-Hubbard model at unit boson filling [38], which has an emergent O(2) quantum critical point separating the Mott insulating and superfluid phases. This critical point features Lorentz invari-

Table I. Leading scaling behaviors of the edge two-point correlation $g(L/2)$ and the superfluid stiffness ρ_s in critical phases.

	$g(L/2)$	ρ_s
special	$L^{-\eta}$, $\eta \approx 0.65$	L^{-1}
KT-like	$L^{-\eta}$, $\eta = 1/4$	L^{-1}
SE-MIB	$L^{-\eta}$, $\eta \in (0, 1/4)$	L^{-1}
ordinary	$L^{-\eta}$, $\eta \approx 2.438$	L^{-1}
extraordinary	$[\ln(L)]^{-\hat{q}}$, $\hat{q} \approx 0.59$	$L^{-1} \ln(L)$

ance with $z = 1$. The present authors and coworkers have given an estimate for the quantum critical point as $t_c = 0.0597291(8)$ [39], which agrees with the literature result $t_c = 0.05974(3)$ [40] and will be adopted to exploit the BCB.

As detailed below, we explore quantum phases of model (5) by FSS and the results are summarized as a ground-state phase diagram in Fig. 1(b). There is a phase, dubbed SE-MIB, that features superfluid edges on top of Mott insulating bulk. Moreover, there are three critical edge phases at t_c : the ordinary, the special, and the extraordinary-log phases. Scaling behaviors of edge critical phases are described in Table I [41].

Methodology. We use the worm quantum Monte Carlo algorithm [42, 43] to simulate model (5) in the imaginary-time path integral representation. The maximum side length of the square lattice is up to $L = 192$. The inverse temperature is set as $\beta = L$, which is in line with $z = 1$. We study the special, the ordinary, and the extraordinary phases at $t = 0.0597291$ by varying κ , and explore the KT-like transition for $t < t_c$. In particular, we exploit the extraordinary phase in a broad parameter regime.

Analyses of the FSS involving $\ln(L)$ may be “notoriously difficult” [44]. We perform the analyses using least-squares fits. Following standard criterion, we prefer the fits with $\chi^2/\text{DF} \sim 1$, where χ^2 is the Chi squared and DF denotes the degree of freedom. We also examine the stability against varying L_{\min} , which represents the minimum side length involved in a fit.

Special transition. We detect the special transition by tuning κ at $t = t_c$. We sample the winding probability $R_{[10]} = \langle \mathcal{R}_{[10]} \rangle$, where $\mathcal{R}_{[10]} = 1$ if there exists at least a particle line winding around the periodic [10] direction of the square lattice. The winding probability is dimensionless and has the FSS scaling function as $R_{[10]} = \tilde{R}_{[10]}(\epsilon L^{y_t})$, where $\epsilon = \kappa - \kappa_c$ represents the deviation from the critical point κ_c , and y_t relates to the correlation length exponent ν by $y_t = 1/\nu$. $R_{[10]}$ is useful in locating critical points [39]. Expanding $\tilde{R}_{[10]}$ and incorporating corrections to scaling, we obtain

$$R_{[10]} = R_{[10]}^c + \sum_j a_j \epsilon^j L^{j y_t} + \sum_m b_m L^{-\omega_m}, \quad (6)$$

where $R_{[10]}^c$ is somewhat universal, a_j ($j = 1, 2, \dots$) and b_m ($m = 1, 2, \dots$) are non-universal, and ω_m represents exponents for corrections. We show $R_{[10]}$ versus κ in Fig. 2(a), where a scaling invariance point is nearly at $\kappa \approx 1.2$. We fit $R_{[10]}$ data with $L = 48, 64, 96, 128$ and 192 to Eq. (6).

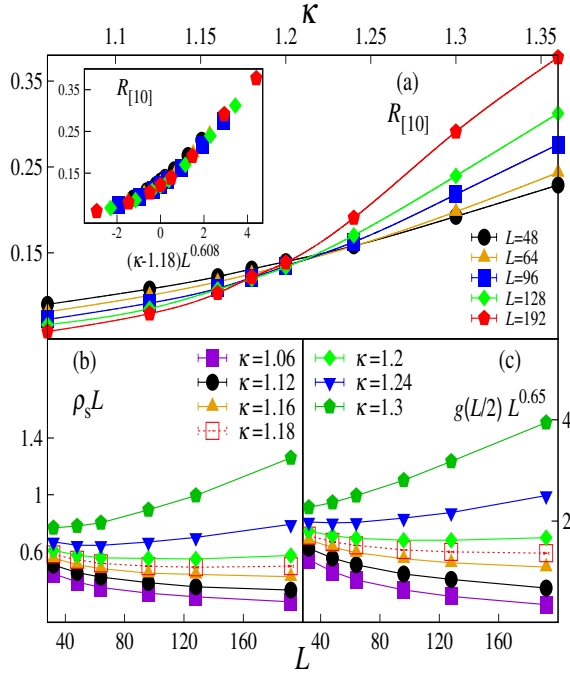


Figure 2. Special transition. (a) Winding probability $R_{[10]}$ versus κ . The inset displays $R_{[10]}$ versus $(\kappa - \kappa_c)L^{y_t}$ with $\kappa_c = 1.18$ and $y_t = 0.608$. (b) Scaled superfluid stiffness $\rho_s L$ versus L . (c) Scaled two-point correlation $g(L/2)L^{4-2y_h}$ with $y_h = 1.675$.

When $b_m = 0$ ($\forall m \geq 1$), we obtain $\kappa_c = 1.206(7)$ and $y_t = 0.44(8)$ with $\chi^2/\text{DF} \approx 4.6$ for $L_{\min} = 64$, $\kappa_c = 1.184(6)$ and $y_t = 0.4(1)$ with $\chi^2/\text{DF} \approx 0.9$ for $L_{\min} = 96$, as well as $\kappa_c = 1.175(5)$ and $y_t = 0.8(3)$ with $\chi^2/\text{DF} \approx 0.2$ for $L_{\min} = 128$. Next, by fixing y_t at the estimate $y_t = 0.608$ for the special transition of classical O(2) model [6], we obtain $\kappa_c = 1.197(2)$, $1.180(3)$ and $1.175(7)$ with $\chi^2/\text{DF} \approx 4.6$, 1.1 and 0.3 , for $L_{\min} = 64$, 96 and 128 , respectively. When $y_t = 0.58$ is fixed, we obtain close estimates, which are detailed in Supplementary Materials (SM). By comparing all these fits, we finally estimate $\kappa_c = 1.18(2)$. For illustrating the single-variable function $\tilde{R}_{[10]}$ together with the estimates of κ_c and y_t , we plot $R_{[10]}$ versus ϵL^{y_t} in Fig. 2(a) with $\kappa_c = 1.18$ and $y_t = 0.608$, where finite-size corrections are already negligible at large systems.

Further evidence is from the FSS of the superfluid stiffness ρ_s , which is defined as [45] $\rho_s = \langle \mathcal{W}_{[10]}^2 \rangle / (2t'\beta)$ through the fluctuations of the winding number $\mathcal{W}_{[10]}$ along the [10] direction of square lattice. At κ_c , ρ_s should scale as $\rho_s \sim L^{2-(d+z)}$. The scaling behavior is verified by Fig. 2(b) with $d = 2$ and $z = 1$: as $L \rightarrow \infty$, $\rho_s L$ is asymptotically a constant for $\kappa \leq \kappa_c$, but bends upwards for $\kappa > \kappa_c$.

We consider the two-point correlation $g(L/2)$ at the largest distance $r_{[10]} = L/2$ along an open edge, which is estimated from the random walks of the two defects in worm quantum Monte Carlo simulations. More descriptions and benchmarks for this estimator are presented in SM. Figure 2(c) shows that the result at κ_c is compatible with the critical scaling behavior

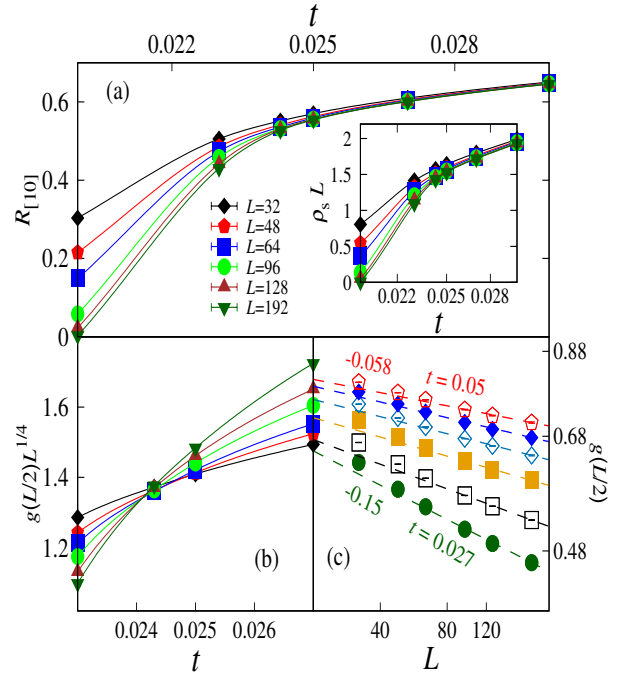


Figure 3. KT-like criticality ($\kappa = 10$). (a) Winding probability $R_{[10]}$ versus t . The inset displays the scaled superfluid stiffness $\rho_s L$. (b) Scaled two-point correlation $g(L/2)L^{1/4}$ versus t . (c) Log-log plot of $g(L/2)$ versus L .

$g(L/2) \sim L^{-0.65}$, yet deviates when $\kappa \neq \kappa_c$. The scaling behavior at κ_c is accounted for by the O(2) special universality with the exponent $y_h = 1.675(1)$ [6], as $g(L/2) \sim L^{2y_h-4}$.

KT-like criticality. Figure 3(a) shows $R_{[10]}$ versus t for $\kappa = 10$. Around $t_c \approx 0.023$, $R_{[10]}$ varies drastically. For $t > t_c$, $R_{[10]}$ extrapolates to a nontrivial value in the $L \rightarrow \infty$ limit, which is dependent of t . Meanwhile, the critical superfluid stiffness scales as $\rho_s \sim L^{-1}$. These observations indicate a regime of critical phase.

The KT-like criticality is evidenced by the anomalous dimension η . Figure 3(b) demonstrates that, at $t_{\text{KT}} \approx t_c$, $g(L/2)$ scales as $g(L/2) \sim L^{2-(d+z)-\eta}$ with $d = 1$, $z = 1$ and $\eta = 1/4$. The value $1/4$ is consistent with that of the KT transition in 2D XY model [46]. For $t > t_{\text{KT}}$, we fit $g(L/2)$ to the formula $g(L/2) \sim L^{-\eta}$ of leading scaling. The fits are illustrated by Fig. 3(c) and detailed in SM. In particular, for $t = 0.027$ and 0.05 , we obtain $\eta = 0.150(2)$ and $0.058(4)$ respectively, with $\chi^2/\text{DF} \approx 1.0$ and $L_{\min} = 96$. The continuously varying exponent η is reminiscent of the low-temperature critical phase of 2D XY model [47].

Ordinary critical phase. Corresponding to classical O(2) BCB, the small- κ side of special transition may fall into an ordinary critical universality class. For $\kappa = 0.4$, Fig. 4 demonstrates that $g(L/2)$ scales as $L^{2-(d+z)-\eta}$ with $\eta \approx 2.438$, $d = 1$ and $z = 1$. The value of η relates to $y_h = 0.781(2)$ [6] of the O(2) BCB by $\eta = 4 - 2y_h$. As $L \rightarrow \infty$, $\rho_s L$ tends to be independent of L . These scaling behaviors indicate the existence of the O(2) quantum ordinary universality.

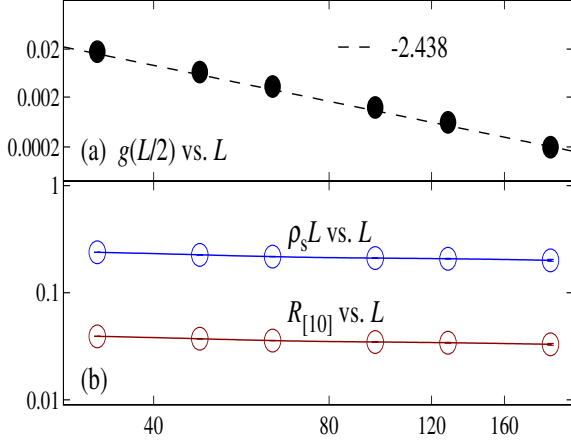


Figure 4. Ordinary critical phase. (a) Log-log plot of two-point correlation $g(L/2)$ versus L for $\kappa = 0.4$. The slope -2.438 relates to $2y_h - 4$ with $y_h = 0.781$. (b) Log-log plot of the scaled superfluid stiffness $\rho_s L$ and the winding probability $R_{[10]}$ versus L .

Extraordinary-log critical phase. For exploring the extraordinary phase, we make use of a broad parameter regime in the large- κ side of special transition. In the ELU, $g(L/2)$ scales as [20]

$$g(L/2) = a[\ln(L/l_0)]^{-\hat{q}}, \quad (7)$$

where l_0 is a reference length and a denotes a non-universal constant. For the classical XY model, this scaling form was verified with the estimate $\hat{q} = 0.59(2)$ [26]. Recently, close values of \hat{q} were obtained for the classical ELU of O(2) model [27] and emergent O(2) criticality [30, 31]. We perform fits for $g(L/2)$ according to Eq. (7), and obtain $0.3 \lesssim \hat{q} \lesssim 0.7$ for $\kappa = 2, 3, 5$ and 7 . We observe that l_0 decreases significantly as κ increases. These features conform with the observations for classical extraordinarily-log universality in Ref. [26]. When $\hat{q} = 0.59$ is fixed, we achieve, for each κ , stable fitting results for l_0 and a . Instance results of l_0 include $l_0 = 0.31(3), 0.21(1), 0.04(4), 0.0108(5)$ and $0.002(1)$, with $\chi^2/\text{DF} \approx 0.3, 1.8, 0.9, 0.7$ and 0.5 , for $\kappa = 2, 3, 5, 7$ and 10 , respectively. The power-law dependence of $g(L/2)$ on $\ln(L/l_0)$ is illustrated by Fig. 5(a).

From Fig. 5(b), we find that the scaled superfluid stiffness $\rho_s L$ roughly obeys the logarithmic scaling formula

$$\rho_s L = b \ln(L) + c \quad (8)$$

with universal $b \approx 1.1$ and non-universal c . Accordingly, we perform fits to $\sum_{\kappa} \rho_s L = 5b \ln(L) + C$ (C is a fitting parameter) where the summation runs over the set $\{2, 3, 5, 7, 10\}$ of κ . For $L_{\min} = 64$, we obtain reasonably good results as $5b = 5.8(2)$ and $C = -5.3(7)$ with $\chi^2/\text{DF} \approx 2.0$ and $L_{\max} = 192$, as well as $5b = 5.6(2)$ and $C = -4.6(8)$ with $\chi^2/\text{DF} \approx 0.8$ and $L_{\max} = 128$. These fits are consistent and finally yield $5b = 5.7(3)$, which relates to $b = 1.14(6)$. By contrast, the logarithmic divergence of $\rho_s L$ is absent in the standard paradigm of criticality, as illustrated for special

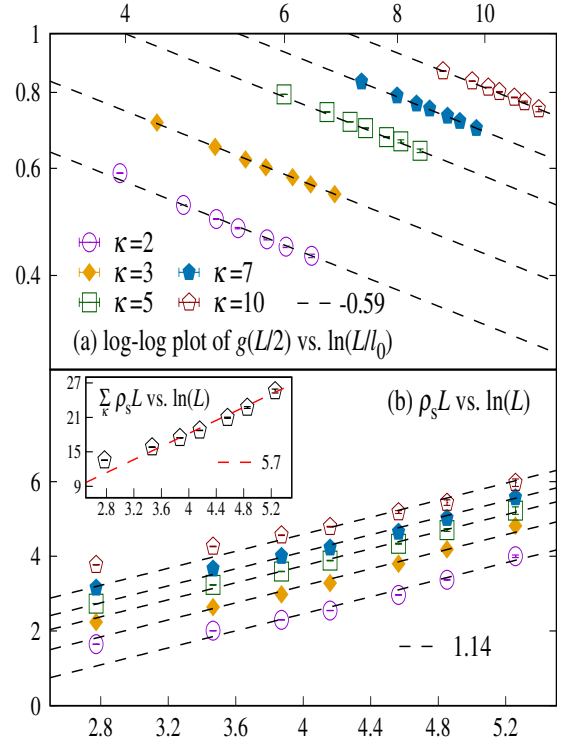


Figure 5. Extraordinary-log critical phase. (a) Log-log plot of two-point correlation $g(L/2)$ versus $\ln(L/l_0)$, where the values of l_0 come from preferred fits. The slope -0.59 relates to $-\hat{q}$. (b) Scaled superfluid stiffness $\rho_s L$ versus $\ln(L)$. Inset: the summation of $\rho_s L$ over κ . The slopes 1.14 and 5.7 denote b in Eq. (8) and $5b$, respectively.

transition [Fig. 2(b)] and ordinary critical phase [Fig. 4(b)], and does not emerge in the KT-like criticality [Fig. 3(a)]. We mention that, the logarithmic FSS (8) with unit exponent and nearly universal coefficient resembles that of the helicity modulus in classical XY and Heisenberg models [20, 25, 26].

Summary. We study the QEC of a 2D Bose-Hubbard model at unit boson filling. We find an edge superfluid phase on top of an insulating bulk. When the bulk is at the emergent quantum critical point, the special, the ordinary and the extraordinary-log critical phases emerge on open edges, each of which admits a one-to-one correspondence to its classical counterpart. In the extraordinary-log critical phase, the leading FSS for largest-distance two-point correlation and scaled superfluid stiffness are logarithmic. By an overall classical-quantum correspondence of O(2) BCB and the universal behavior of logarithmic FSS in extraordinary phase, we provide complementary evidence for the quantum ELU, which has been intensively pursued. As the Bose-Hubbard model can be accessed by the quantum emulators with ultracold bosons in optical lattices [48–51], our findings might be experimentally testable.

Acknowledgments. One of us (J.P.L.) wishes to warmly thank Prof. Youjin Deng for the collaboration in an earlier related work [26]. The present work has been supported by the

- [1] K. Binder and P. C. Hohenberg, “Surface effects on magnetic phase transitions,” *Phys. Rev. B* **9**, 2194 (1974).
- [2] K. Ohno and Y. Okabe, “The $1/n$ expansion for the extraordinary transition of semi-infinite system,” *Prog. Theor. Phys.* **72**, 736–745 (1984).
- [3] D. P. Landau, R. Pandey, and K. Binder, “Monte carlo study of surface critical behavior in the xy model,” *Phys. Rev. B* **39**, 12302 (1989).
- [4] H. W. Diehl, “The theory of boundary critical phenomena,” *Int. J. Mod. Phys. B* **11**, 3503–3523 (1997), arXiv:cond-mat/9610143 [cond-mat].
- [5] M. Pleimling, “Critical phenomena at perfect and non-perfect surfaces,” *J. Phys. A: Math. and Gen.* **37**, R79 (2004), arXiv:cond-mat/0402574 [cond-mat].
- [6] Y. Deng, H. W. J. Blöte, and M. P. Nightingale, “Surface and bulk transitions in three-dimensional $o(n)$ models,” *Phys. Rev. E* **72**, 016128 (2005), arXiv:cond-mat/0504173 [cond-mat].
- [7] Y. Deng, “Bulk and surface phase transitions in the three-dimensional $o(4)$ spin model,” *Phys. Rev. E* **73**, 056116 (2006).
- [8] J. Dubail, J. L. Jacobsen, and H. Saleur, “Exact solution of the anisotropic special transition in the $o(n)$ model in two dimensions,” *Phys. Rev. Lett.* **103**, 145701 (2009), arXiv:0909.2949 [cond-mat].
- [9] L. Zhang and F. Wang, “Unconventional surface critical behavior induced by a quantum phase transition from the two-dimensional affleck-kennedy-lieb-tasaki phase to a néel-ordered phase,” *Phys. Rev. Lett.* **118**, 087201 (2017), arXiv:1611.06477 [cond-mat].
- [10] C. Ding, L. Zhang, and W. Guo, “Engineering surface critical behavior of $(2+1)$ -dimensional $o(3)$ quantum critical points,” *Phys. Rev. Lett.* **120**, 235701 (2018), arXiv:1801.10035 [cond-mat].
- [11] L. Weber, F. Parisen Toldin, and S. Wessel, “Nonordinary edge criticality of two-dimensional quantum critical magnets,” *Phys. Rev. B* **98**, 140403(R) (2018), arXiv:1804.06820 [cond-mat].
- [12] L. Weber and S. Wessel, “Nonordinary criticality at the edges of planar spin-1 heisenberg antiferromagnets,” *Phys. Rev. B* **100**, 054437 (2019), arXiv:1906.07051 [cond-mat].
- [13] T. Grover and A. Vishwanath, “Quantum criticality in topological insulators and superconductors: Emergence of strongly coupled majoranas and supersymmetry,” arXiv:1206.1332 [cond-mat].
- [14] D. E. Parker, T. Scaffidi, and R. Vasseur, “Topological luttinger liquids from decorated domain walls,” *Phys. Rev. B* **97**, 165114 (2018), arXiv:1711.09106 [cond-mat].
- [15] S. Liu, H. Shapourian, A. Vishwanath, and M. A. Metlitski, “Magnetic impurities at quantum critical points: Large- n expansion and connections to symmetry-protected topological states,” *Phys. Rev. B* **104**, 104201 (2021), arXiv:2104.15026 [cond-mat].
- [16] D. M. Dantchev and S. Dietrich, “Critical casimir effect: Exact results,” arXiv:2203.15050 [cond-mat].
- [17] J. Cardy, “Boundary conformal field theory,” arXiv:hep-th/0411189 [cond-mat].
- [18] D. Poland, S. Rychkov, and A. Vichi, “The conformal bootstrap: Theory, numerical techniques, and applications,” *Rev. Mod. Phys.* **91**, 015002 (2019), arXiv:1805.04405 [cond-mat].
- [19] N. Andrei, A. Bissi, M. Buican, J. Cardy, P. Dorey, N. Drukker, J. Erdmenger, D. Friedan, D. Fursaev, A. Konechny, C. Kristjansen, I. Makabe, Y. Nakayama, A. O’Bannon, R. Parini, B. Robinson, S. Ryu, C. Schmidt-Colinet, V. Schomerus, C. Schweigert, and G. M. T. Watts, “Boundary and defect CFT: open problems and applications,” *J. Phys. A: Math. and Theo.* **53**, 453002 (2020), arXiv:1810.05697 [cond-mat].
- [20] Metlitski M. A., “Boundary criticality of the $o(n)$ model in $d=3$ critically revisited,” *SciPost Phys.* **12**, 131 (2022), arXiv:2009.05119 [cond-mat].
- [21] S. Sachdev, *Quantum phase transitions* (Wiley Online Library, 2007).
- [22] R. Fernández, J. Fröhlich, and A. D. Sokal, *Random walks, critical phenomena, and trivality in quantum field theory* (Springer, Berlin, 2013).
- [23] A. Goldman, *Percolation, localization, and superconductivity*, Vol. 109 (Springer, Boston, 2013).
- [24] B. V. Svistunov, E. S. Babaev, and N. V. Prokof’ev, *Superfluid states of matter* (CRC Press, London, 2015).
- [25] F. Parisen Toldin, “Boundary critical behavior of the three-dimensional heisenberg universality class,” *Phys. Rev. Lett.* **126**, 135701 (2021), arXiv:2012.00039 [cond-mat].
- [26] M. Hu, Y. Deng, and J.-P. Lv, “Extraordinary-log surface phase transition in the three-dimensional xy model,” *Phys. Rev. Lett.* **127**, 120603 (2021), arXiv:2104.05152 [cond-mat].
- [27] J. Padayasi, A. Krishnan, M. A. Metlitski, I. A. Gruzberg, and M. Meineri, “The extraordinary boundary transition in the 3d $o(n)$ model via conformal bootstrap,” arXiv:2111.03071 [cond-mat].
- [28] F. Parisen Toldin and M. A. Metlitski, “Boundary criticality of the 3d $o(n)$ model: from normal to extraordinary,” arXiv:2111.03613 [cond-mat].
- [29] F. Parisen Toldin, “Surface critical behavior of the three-dimensional $o(3)$ model,” arXiv:2111.11762 [cond-mat].
- [30] L.-R. Zhang, C. Ding, Y. Deng, and L. Zhang, “Surface criticality of antiferromagnetic potts model,” arXiv:2204.11692 [cond-mat].
- [31] X. Zou, S. Liu, and W. Guo, “Surface critical properties of the three-dimensional clock model,” arXiv:2204.13612 [cond-mat].
- [32] L. Weber and S. Wessel, “Spin versus bond correlations along dangling edges of quantum critical magnets,” *Phys. Rev. B* **103**, L020406 (2021), arXiv:2010.15691 [cond-mat].
- [33] C. Ding, W. Zhu, W. Guo, and L. Zhang, “Special transition and extraordinary phase on the surface of a $(2+1)$ -dimensional quantum heisenberg antiferromagnet,” arXiv:2110.04762 [cond-mat].
- [34] W. Zhu, C. Ding, L. Zhang, and Guo W., “Exotic surface behaviors induced by geometrical settings of two-dimensional dimerized quantum xxz model,” arXiv:2111.12336 [cond-mat].
- [35] X.-J. Yu, R.-Z. Huang, H.-H. Song, L. Xu, C. Ding, and L. Zhang, “Conformal boundary conditions of symmetry-enriched quantum critical spin chains,” arXiv:2111.10945 [cond-mat].
- [36] Y. Xu, Z. Xiong, and L. Zhang, “Persistent corner spin mode at the quantum critical point of a plaquette heisenberg model,” arXiv:2112.04616 [cond-mat].
- [37] C.-M. Jian, Y. Xu, X.-C. Wu, and C. Xu, “Continuous neel-vbs quantum phase transition in non-local one-dimensional sys-

- tems with $so(3)$ symmetry,” *SciPost Physics* **10**, 033 (2021), [arXiv:2004.07852 \[cond-mat\]](#).
- [38] M. P. A. Fisher, P. B. Weichman, G. Grinstein, and D. S. Fisher, “Boson localization and the superfluid-insulator transition,” *Phys. Rev. B* **40**, 546–570 (1989).
- [39] W. Xu, Y. Sun, J.-P. Lv, and Y. Deng, “High-precision monte carlo study of several models in the three-dimensional $u(1)$ universality class,” *Phys. Rev. B* **100**, 064525 (2019), [arXiv:1908.10990 \[cond-mat\]](#).
- [40] B. Capogrosso-Sansone, S. G. Soyler, N. Prokof’ev, and B. Svistunov, “Monte carlo study of the two-dimensional bose-hubbard model,” *Phys. Rev. A* **77**, 015602 (2008), [arXiv:0710.2703 \[cond-mat\]](#).
- [41] Logarithmic corrections may emerge for the KT-like transition and the SE-MIB phase [47].
- [42] N. V. Prokof’ev, B. V. Svistunov, and I. S. Tupitsyn, “Exact, complete, and universal continuous-time worldline monte carlo approach to the statistics of discrete quantum systems,” *Sov. Phys. JETP* **87**, 310–321 (1998), [arXiv:cond-mat/9703200 \[cond-mat\]](#).
- [43] N. V. Prokof’ev, B. V. Svistunov, and I. S. Tupitsyn, ““worm” algorithm in quantum monte carlo simulations,” *Phys. Lett. A* **238**, 253–257 (1998).
- [44] P. Grassberger, “Critical percolation in high dimensions,” *Phys. Rev. E* **67**, 036101 (2003), [arXiv:cond-mat/0202144 \[cond-mat\]](#).
- [45] E. L. Pollock and D. M. Ceperley, “Path-integral computation of superfluid densities,” *Phys. Rev. B* **36**, 8343–8352 (1987).
- [46] J. M. Kosterlitz, “The critical properties of the two-dimensional xy model,” *J. Phys. C: Solid State Phys.* **7**, 1046 (1974).
- [47] J. M. Kosterlitz, “Kosterlitz–thouless physics: a review of key issues,” *Rep. Prog. Phys.* **79**, 026001 (2016).
- [48] D. Jaksch, C. Bruder, J. I. Cirac, C. W. Gardiner, and P. Zoller, “Cold bosonic atoms in optical lattices,” *Phys. Rev. Lett.* **81**, 3108 (1998), [arXiv:cond-mat/9805329 \[cond-mat\]](#).
- [49] M. Greiner, O. Mandel, T. Esslinger, T. W. Hänsch, and I. Bloch, “Quantum phase transition from a superfluid to a mott insulator in a gas of ultracold atoms,” *Nature* **415**, 39–44 (2002).
- [50] S. Baier, M. J. Mark, D. Petter, K. Aikawa, L. Chomaz, Z. Cai, M. Baranov, P. Zoller, and F. Ferlaino, “Extended bose-hubbard models with ultracold magnetic atoms,” *Science* **352**, 201–205 (2016), [arXiv:1507.03500 \[cond-mat\]](#).
- [51] B. Yang, H. Sun, C.-J. Huang, H.-Y. Wang, Y. Deng, H.-N. Dai, Z.-S. Yuan, and J.-W. Pan, “Cooling and entangling ultracold atoms in optical lattices,” *Science* **369**, 550–553 (2020), [arXiv:1901.01146 \[cond-mat\]](#).

Supplementary Materials for “Quantum extraordinary-log universality of boundary critical behavior”

Yanan Sun¹ and Jian-Ping Lv^{1,*}

¹*Department of Physics and Anhui Key Laboratory of Optoelectric Materials Science and Technology,
Key Laboratory of Functional Molecular Solids, Ministry of Education,
Anhui Normal University, Wuhu, Anhui 241000, China*

Here, we present details for Monte Carlo simulations and provide a benchmark for two-point correlation using bulk criticality. We then analyze the data for the quantum critical phenomena on open edges, which include the special transition, the Kosterlitz-Thouless-like criticality, the ordinary critical phase and the extraordinary-log critical phase.

The raw data are all obtained from quantum Monte Carlo simulations, by means of the worm algorithm in the continuous-time path integral representation. The side lengths of the square lattices include $L = 16, 32, 48, 64, 96, 128$ and 192 . In the worm simulations, the number of tentative updates for the defects, usually denoted by *Ira* (I) and *Masha* (M), ranges from 3.6×10^{12} to 3.4×10^{13} for $16 \leq L \leq 48$, and from 1.8×10^{13} to 3.7×10^{13} for $64 \leq L \leq 192$.

We perform finite-size scaling (FSS) analyses by using least-squares fits. To this end, we utilize the function `NonlinearModelFit` in Mathematica, as adopted in Ref. [1]. According to standard criterion, we prefer the fits with $\chi^2/\text{DF} \sim 1$, where χ^2/DF represents the Chi squared per degree of freedom. We conclude by comparing the fits that are stable against varying L_{\min} , which is the minimum side length incorporated in a fit. In certain situations, we also include a cutoff L_{\max} for larger sizes.

I. BENCHMARK FOR TWO-POINT CORRELATION USING BULK CRITICALITY

We use an estimator of equal-imaginary-time correlations, which avoids reweighting along imaginary-time axis and turns out to be computationally cheap. The estimator correctly captures the asymptotic behavior in the $L \rightarrow \infty$ limit. Specifically speaking, in the worm quantum Monte Carlo simulations, we trace the trajectories of the defects *I* and *M* on an edge. If the imaginary-time distance between the defects is less than the $1/L$ fraction of entire axis, the distance r of two defects along the edge is recorded. The follow-up treatment is similar to the measurement of two-point correlations in a classical model [2] which was based on the original idea in Ref. [3]. We use the $r = 1$ result to normalize the two-point correlation and concentrate on the $r \neq 0$ domain of correlation function. Hence, the results do not suffer from the biased allocations of statistical weight between original and Green function state spaces. Finally, we obtain the two-point correlation $g(r)$ as a function of r along the edge.

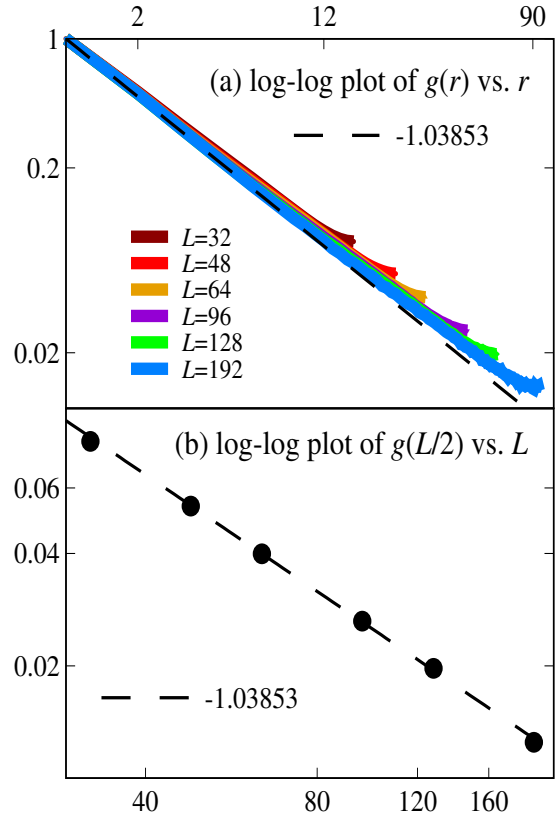


Figure 1. Bulk critical point. (a) Log-log plot of $g(r)$ versus r . (b) Log-log plot of $g(L/2)$ versus L .

We proceed to benchmark the above-mentioned methodology for correlation function using the bulk criticality. Particularly, we apply periodic conditions for both [10] and [01] directions to eliminate the open edges and sample the correlation functions at t_c . We analyze the r dependence of $g(r)$ as well as the L -dependent behavior of $g(L/2)$. We quote a precise estimate $\eta = 0.03853(48)$ for the anomalous dimension of the (2+1)-dimensional $O(2)$ criticality [4]. As shown in Fig. 1(a), the r -dependent behavior converges to the power law $g(r) \sim r^{2-(d+z)-\eta}$, with $d = 2$, $z = 1$ and $\eta \approx 0.03853$. From Fig. 1(b), we verify that $g(L/2)$ scales as $g(L/2) \sim L^{-1.03853}$.

More quantitative verification can be achieved by least-squares fits. We fit $g(L/2)$ to

$$g(L/2) = aL^b, \quad (1)$$

* jplv2014@ahnu.edu.cn

Table I. Fits of $g(L/2)$ to Eq. (1) at the bulk critical point.

L_{\min}	χ^2/DF	a	b
32	20.62/4	2.65(3)	-1.009(3)
48	3.45/3	2.86(6)	-1.027(6)
64	3.04/2	2.9(1)	-1.03(1)
96	1.41/1	3.4(4)	-1.06(3)

where a is a constant and $b = -1 - \eta$. The results are summarized in Table I. We obtain $b = -1.027(6)$ and $\chi^2/\text{DF} \approx 1.2$ for $L_{\min} = 48$, $b = -1.03(1)$ and $\chi^2/\text{DF} \approx 1.5$ for $L_{\min} = 64$, as well as $b = -1.06(3)$ and $\chi^2/\text{DF} \approx 1.4$ for $L_{\min} = 96$. The estimates of b are consistent with $-1 - \eta = -1.03853(48)$ of the (2+1)-dimensional O(2) universality.

II. CRITICAL PHENOMENA ON OPEN EDGES

In this section, we perform FSS analyses for the special transition, the Kosterlitz-Thouless-like criticality, the ordinary critical phase and the extraordinary-log critical phase.

Special transition. We locate the special transition point by the FSS of the winding probability $R_{[10]}$. We perform fits according to

$$R_{[10]} = R_{[10]}^c + a_1(\kappa - \kappa_c)L^{y_t}, \quad (2)$$

where $R_{[10]}^c$ is the critical dimensionless ratio, a_1 represents a fitting parameter, κ_c denotes the transition point, and y_t relates to the correlation length exponent ν by $y_t = 1/\nu$. We perform least-squares fits with $\kappa = 1.16, 1.18, 1.2$ and $L = 48, 64, 96, 128, 192$, and obtain reasonably good results for large L_{\min} . We also perform fits by fixing y_t at 0.608 and 0.58, which were estimated for the special transition in classical O(2) models in spin [5] and flow representation [6], respectively. The results are listed in Table II. By comparing the fits, our final estimate of κ_c is $\kappa_c = 1.18(2)$.

Kosterlitz-Thouless-like criticality. We explore the critical phase at the large- t side of the Kosterlitz-Thouless-like transition for $\kappa = 10$. For each t in the set $\{0.027, 0.03, 0.035, 0.04, 0.045, 0.05\}$, we perform scaling analyses for $g(L/2)$ according to Eq. (1) with $b = -\eta$, which captures the leading FSS, and the results are summarized in Table III. The fits are precise only at large sizes. Moreover, as t increases, the exponent η decreases.

Ordinary critical phase. We consider the ordinary critical phase with the hopping enhancement $\kappa = 0.4$ at t_c . We analyze $g(L/2)$ by Eq. (1) with $b = 2y_h - 4$. The results are presented in Table IV. For $L_{\min} = 48, 64$ and 96 , we find $b = -2.41(2), -2.45(4)$ and $-2.5(1)$, with $\chi^2/\text{DF} \approx 1.3, 1.1$ and 1.4 , respectively. These results are compatible with the exponent $2y_h - 4$ with $y_h = 0.781(2)$ of the classical O(2) ordinary surface criticality [5].

Extraordinary critical phase. We analyze the FSS for the extraordinary phase. We fit $g(L/2)$ to

$$g(L/2) = a[\ln(L/l_0)]^{-\hat{q}}, \quad (3)$$

and the results are listed in Table V. If \hat{q} is free, we obtain $0.3 \lesssim \hat{q} \lesssim 0.7$, and find the tendency that l_0 drastically decreases upon increasing κ . To suppress uncertainty, we fix $\hat{q} = 0.59$. For each considered κ , we obtain stable fitting results of a and l_0 . For l_0 , instance results are $l_0 = 0.31(3), 0.21(1), 0.04(4), 0.0108(5)$ and $0.002(1)$ with $\chi^2/\text{DF} \approx 0.3, 1.8, 0.9, 0.7$ and 0.5 , for $\kappa = 2, 3, 5, 7$ and 10 , respectively.

Assuming a unique critical universality for the extraordinary phase, we analyze the sum of scaled superfluid stiffness $\rho_s L$ over $\kappa = 2, 3, 5, 7$ and 10 by performing fits to

$$\sum_{\kappa} \rho_s L = A + B \ln L. \quad (4)$$

As summarized in Table VI, we obtain reasonably good fits with $\chi^2/\text{DF} \sim 1$ for $L_{\max} = 192$ and 128 . For $L_{\max} = 192$, we obtain $A = -5.3(7), B = 5.8(2)$ and $\chi^2/\text{DF} \approx 2.0$ with $L_{\min} = 64$, as well as $A = -8.8(2.0), B = 6.5(4)$ and $\chi^2/\text{DF} \approx 0.5$ with $L_{\min} = 96$. For $L_{\max} = 128$, we obtain $A = -4.6(8), B = 5.6(2)$ and $\chi^2/\text{DF} \approx 0.8$ with $L_{\min} = 64$.

-
- [1] J. Salas, "Phase diagram for the bisected-hexagonal-lattice five-state potts antiferromagnet," *Phys. Rev. E* **102**, 032124 (2020), [arXiv:2006.04866 \[cond-mat\]](#).
- [2] J.-P. Lv, W. Xu, Y. Sun, K. Chen, and Y. Deng, "Finite-size scaling of o(n) systems at the upper critical dimensionality," *Natl. Sci. Rev.* **8**, nwaa212 (2021), [arXiv:1909.10347 \[cond-mat\]](#).
- [3] N. Prokof'ev and B. Svistunov, "Worm algorithms for classical statistical models," *Phys. Rev. Lett.* **87**, 160601 (2001),

- [arXiv:cond-mat/0103146 \[cond-mat\]](#).
- [4] W. Xu, Y. Sun, J.-P. Lv, and Y. Deng, "High-precision monte carlo study of several models in the three-dimensional u(1) universality class," *Phys. Rev. B* **100**, 064525 (2019), [arXiv:1908.10990 \[cond-mat\]](#).
- [5] Y. Deng, H. W. J. Blöte, and M. P. Nightingale, "Surface and bulk transitions in three-dimensional o(n) models," *Phys. Rev. E* **72**, 016128 (2005), [arXiv:cond-mat/0504173 \[cond-mat\]](#).
- [6] Y. Sun, J. Lyu, and J.-P. Lv, "unpublished result," (2021).

Table II. Fits of $R_{[10]}$ to Eq. (2) for the special transition.

L_{\min}	χ^2/DF	κ_c	y_t	$R_{[10]}^c$	a_1
48	108.12/11	1.25(1)	0.29(5)	0.160(7)	0.15(3)
64	37.02/8	1.206(7)	0.44(8)	0.138(4)	0.08(3)
96	4.41/5	1.184(6)	0.4(1)	0.123(4)	0.10(7)
128	0.33/2	1.175(5)	0.8(3)	0.117(4)	0.01(2)
48	145.25/12	1.206(2)	0.608	0.1398(8)	0.0394(9)
64	41.39/9	1.197(2)	0.608	0.133(1)	0.037(1)
96	6.35/6	1.180(3)	0.608	0.121(2)	0.038(1)
128	0.84/3	1.175(7)	0.608	0.116(5)	0.035(2)
48	138.73/12	1.208(2)	0.58	0.1407(8)	0.045(1)
64	40.01/9	1.198(2)	0.58	0.134(1)	0.042(1)
96	5.84/6	1.181(4)	0.58	0.121(2)	0.043(2)
128	0.98/3	1.175(7)	0.58	0.116(5)	0.040(2)

Table III. Fits of $g(L/2)$ to Eq. (1) for the large- t side of Kosterlitz-Thouless-like transition at $\kappa = 10$.

t	L_{\min}	χ^2/DF	a	b
0.027	48	208.63/3	1.115(3)	-0.1700(6)
	64	36.28/2	1.080(4)	-0.1628(8)
	96	0.96/1	1.01(1)	-0.150(2)
0.03	48	591.62/3	1.016(2)	-0.1264(4)
	64	127.87/2	0.980(2)	-0.1187(5)
	96	6.02/1	0.929(5)	-0.108(1)
0.035	48	437.57/3	0.990(1)	-0.0979(3)
	64	119.14/2	0.964(2)	-0.0924(4)
	96	5.54/1	0.925(4)	-0.0841(9)
0.04	48	96.45/3	1.010(2)	-0.0881(5)
	64	28.96/2	0.991(3)	-0.0839(7)
	96	0.65/1	0.950(8)	-0.075(2)
0.045	48	24.06/3	1.017(3)	-0.0788(7)
	64	6.70/2	1.003(4)	-0.076(1)
	96	1.05/1	0.97(1)	-0.069(3)
0.05	48	18.18/3	1.017(4)	-0.070(1)
	64	9.31/2	1.004(6)	-0.067(1)
	96	0.98/1	0.96(2)	-0.058(4)

Table IV. Fits of $g(L/2)$ to Eq. (1) for the ordinary critical phase at $\kappa = 0.4$.

L_{\max}	L_{\min}	χ^2/DF	a	b
192	32	7.02/4	66.6(1.8)	-2.374(7)
	48	4.01/3	76.5(6.5)	-2.41(2)
	64	2.15/2	90.9(14.1)	-2.45(4)
	96	1.41/1	141.2(77.8)	-2.5(1)
128	32	2.62/3	66.2(1.8)	-2.373(7)
	48	0.84/2	73.9(6.4)	-2.40(2)
	64	0.002/1	83.7(13.7)	-2.43(4)

Table V. Fits of $g(L/2)$ to Eq. (3) for the extraordinary phase at $\kappa = 2, 3, 5, 7$ and 10 .

κ	L_{\min}	χ^2/DF	a	l_0	\hat{q}
2	16	1.93/4	0.68(1)	3.5(3)	0.32(1)
	32	0.12/3	0.76(8)	2.2(9)	0.38(5)
	48	0.07/2	0.7(2)	3.3(4.9)	0.3(2)
	64	0.03/1	0.8(9)	1.7(8.1)	0.4(5)
	16	177.76/5	1.170(2)	0.648(8)	0.59
	32	8.09/4	1.248(7)	0.40(2)	0.59
	48	0.89/3	1.29(2)	0.31(3)	0.59
	64	0.12/2	1.31(4)	0.25(7)	0.59
	96	0.07/1	1.33(8)	0.2(1)	0.59
3	16	2.74/4	1.11(8)	1.0(2)	0.42(3)
	32	1.01/3	0.9(1)	2.3(1.3)	0.33(6)
	48	0.42/2	1.5(2.0)	0.3(1.2)	0.5(5)
	16	16.72/5	1.649(3)	0.257(4)	0.59
	32	7.21/4	1.69(1)	0.21(1)	0.59
	48	0.42/3	1.73(2)	0.16(2)	0.59
	64	0.31/2	1.75(5)	0.15(4)	0.59
	96	0.003/1	1.7(1)	0.2(2)	0.59
5	16	2.17/4	2.7(9)	0.03(3)	0.7(1)
	32	1.30/3	1.5(6)	0.3(5)	0.5(2)
	48	1.14/2	2.7(6.5)	0.02(22)	0.7(8)
	64	0.99/1	1.1(1.3)	1.2(7.4)	0.3(5)
	16	2.57/5	2.221(6)	0.053(1)	0.59
	32	1.72/4	2.20(2)	0.058(5)	0.59
	48	1.15/3	2.23(4)	0.05(1)	0.59
	64	1.08/2	2.21(7)	0.05(2)	0.59
	96	0.85/1	2.3(2)	0.04(4)	0.59
7	16	2.29/4	4.4(2.7)	0.001(4)	0.7(2)
	32	1.34/3	1.7(9)	0.1(3)	0.4(2)
	16	3.31/5	2.692(9)	0.0108(5)	0.59
	32	1.67/4	2.66(3)	0.013(2)	0.59
	48	0.83/3	2.70(5)	0.010(3)	0.59
	64	0.06/2	2.63(9)	0.015(7)	0.59
	96	0.001/1	2.6(2)	0.02(2)	0.59
	10	16	12.53/5	3.35(2)	0.00084(8)
32		0.93/4	3.22(4)	0.0017(4)	0.59
48		0.91/3	3.21(8)	0.0018(7)	0.59
64		0.91/2	3.2(1)	0.002(1)	0.59
96		0.08/1	3.0(3)	0.01(1)	0.59

Table VI. Fits of the summed scaled stiffness $\sum \rho_s L$ over $\kappa = 2, 3, 5, 7$ and 10 to Eq. (4) for the extraordinary phase.

L_{\max}	L_{\min}	χ^2/DF	A	B
192	32	95.84/4	0.2(2)	4.47(5)
	48	28.71/3	-2.3(4)	5.10(9)
	64	3.98/2	-5.3(7)	5.8(2)
	96	0.45/1	-8.8(2.0)	6.5(4)
128	32	64.32/3	0.5(2)	4.41(5)
	48	16.33/2	-1.9(4)	5.0(1)
	64	0.77/1	-4.6(8)	5.6(2)